Measurement of GPS Antenna Gain Patterns for CYGNSS Using a Spaceborne Antenna Range

TIANLIN WANG, Senior Member, IEEE
The Ohio State University, Columbus, OH USA

CHRISTOPHER S. RUF, Life Fellow, IEEE
University of Michigan, Ann Arbor, MI USA

ANDREW J. O'BRIEN

SCOTT GLEASON, Senior Member, IEEE
Daaxa LLC, Boulder, CO USA

DARREN S. MCKAGUE, Member, IEEE
BRUCE P. BLOCK
ANTHONY RUSSEL
University of Michigan, Ann Arbor, MI USA

Manuscript received 21 April 2023; revised 14 December 2023 and 23 May 2024; accepted 28 May 2024. Date of publication 14 June 2024; date of current version 11 October 2024.

DOI. No. 10.1109/TAES.2024.3414961

Refereeing of this contribution was handled by S. Khanafseh.

This work was supported in part by the NASA Science Mission Directorate under Contract NNL13AQ00C with the University of Michigan and in part by The Ohio State University President's Postdoctoral Scholars Fellowship.

Authors' addresses: Tianlin Wang is with the Department of Electrical and Computer Engineering and ElectroScience Laboratory, The Ohio State University, Columbus, OH 43210 USA, E-mail: (wang.15085@osu.edu); Christopher S. Ruf is with the Department of Climate and Space Sciences and Engineering, University of Michigan, Ann Arbor, MI 48109 USA, E-mail: (cruf@umich.edu); Andrew J. O'Brien was with the ElectroScience Laboratory, Department of Electrical and Computer Engineering, The Ohio State University, Columbus, OH 43210, USA, E-mail: (andrew.obrien.200@gmail.com); Scott Gleason are with Daaxa LLC, Boulder, CO 80305 USA, E-mail: (sgleason@protonmail.com); Darren S. McKague is with the Department of Climate and Space Sciences and Engineering, University of Michigan, Ann Arbor, MI 48109 USA, E-mail: (dmckague@umich.edu); Bruce P. Block and Anthony Russel are with the Space Physics Research Laboratory, University of Michigan, Ann Arbor, MI 48109 USA, E-mail: (bpblock@umich.edu; russelan@umich.edu). *(Corresponding author: Tianlin Wang.)*

© 2024 The Authors. This work is licensed under a Creative Commons Attribution-NonCommercial-NoDerivatives 4.0 License. For more information, see https://creativecommons.org/licenses/by-nc-nd/4.0/

The NASA Cyclone Global Navigation Satellite System (CYGNSS) mission is a constellation of eight small satellites that receive global positioning system (GPS) signals reflected off the earth to support a variety of science applications. For remote sensing, the strength of the reflected GPS signal contains important information and must be known to a small fraction of a dB. This makes it very different from traditional GPS navigation applications, in which small amplitude variations have minor or negligible impact depending on the accuracy requirements of the specific application. Satisfying mission requirements necessitates precise knowledge of the GPS satellite transmit antenna pattern and the receive antenna pattern on each CYGNSS satellite. In this article, we present the antenna calibration approach that is used by the CYGNSS science operations center. GPS satellite and CYGNSS satellite antenna patterns are jointly estimated using several years of on-orbit CYGNSS measurements. The orbiting GPS transmit and CYGNSS receive antennas form a spaceborne antenna measurement range, which can be utilized to determine their patterns. The accuracy of the estimated antenna patterns can then be quantified using CYGNSS GPS science data as a metric. When compared to the limited publicly available GPS satellite antenna data or antenna chamber measurements of the CYGNSS satellites, the proposed on-orbit approach is able to introduce corrections that significantly improve the CYGNSS mission science performance.

I. INTRODUCTION

The global navigation satellite system (GNSS) is the generic term used for constellations of navigation satellites that provide positioning, navigation, and timing (PNT) services on a global basis. The GNSS is currently used in many applications, including navigation, surveying, mapping, and remote sensing [1], [2]. Each GNSS satellite continuously transmits radio frequency (RF) signals toward the earth, which propagates and is then captured by the receiver system, which could be either ground-based, airborne, or spaceborne. The power level of received GNSS signals on the earth is extremely low, typically –160 dBW for the global positioning system (GPS). The signal structure allows a receiver to extract the signal buried in background RF noise and make precise PNT measurements [2]. The GPS satellite transmit antenna is designed to be right-handed circular polarization (RHCP), although the polarization purity of the pattern has not been made publicly available nor published in open literature.

Global navigation satellite system reflectometry (GNSS-R) uses reflected GNSS signals for earth remote sensing applications [3], [4]. Calibration of its delay–Doppler map (DDM) measurements of surface scattering cross section requires knowledge of the effective isotropic radiated power (EIRP) of the GNSS transmitter, e.g., GPS [5]. This, in turn, requires knowledge of the GPS transmit power level and the GPS transmit antenna gain pattern. For the NASA Cyclone Global Navigation Satellite System (CYGNSS) GNSS-R mission [6], [7], DDM calibration is accomplished by its Level 1 calibration algorithm [8], [9]. Changes in GPS transmit power are tracked by real-time monitoring of the power level of direct signals received by the navigation receiver on each CYGNSS spacecraft [10], [11]. The GPS transmit antenna pattern can also be determined from the same direct signals. In addition, the direct signal measurements allow for the determination of the receive antenna patterns on each

TABLE I
GPS and CYGNSS Constellation

Constellation	GPS	CYGNSS
Orbit	MEO	LEO
Height (km)	20,180	~ 520
Inclination (°)	55	35
Period	11 h 58 min	~95 minutes
Number of satellites	31 active	8
Block type	IIR, IIR-M, IIF, and III	Uniform

CYGNSS spacecraft. The work presented here describes how both the patterns are derived from a large collection of direct signal measurements made by the constellation of CYGNSS spacecraft.

The first published GPS *L*-band RHCP antenna patterns included four azimuthal cuts of the relative gain from a Block IIA antenna [12]. Measurements from the Radio Amateur Satellite Corporation (AMSAT) experiment showed that the main lobes on the Block IIR satellites were slightly narrower than those on the Block II/IIA patterns and that some sidelobe levels for Block IIR satellites were significantly higher than expected [13]. This demonstrated that the gain pattern could be significantly affected by the space vehicle (SV) on which it was mounted. Over the next two decades, the publicly available GPS antenna patterns are the measurements for satellites collected during prelaunch testing and published on the GPS Technical Reference website [14]. However, these patterns either only have coarse resolution (2° in off-boresight, and 10° in azimuth) or only include an azimuthally averaged cut, instead of the full antenna pattern. The published patterns by Lockheed Martin [15] have been used to determine the transmit power of GPS satellites in various ground-based experiments [16], [17], [18]. Note that cross-polarization (cross-pol) information is not provided in these published patterns, which were assumed to be purely RHCP. Azimuthal asymmetry in the patterns has been observed by these experiments. Additional studies have shown that the published prelaunch patterns are not of sufficient accuracy to meet the requirements of some GNSS-R scientific investigations [19].

The on-orbit determination of GPS transmit antenna gain patterns was attempted previously by the GPS Antenna Characterization Experiment (ACE), a research collaboration between the Aerospace Corporation and the NASA Goddard Space Flight Center. The GPS ACE characterized the sidelobe portion of GPS L1 antenna patterns using receivers in a geosynchronous equatorial orbit (GEO) [20]. Notably, the main beam (on-earth) portion of the GPS antenna pattern was not characterized, and the patterns were assumed to be purely RHCP.

The work presented here expands upon the approach initially developed by the GPS ACE using GPS receivers deployed on the constellation of CYGNSS satellites in the low earth orbit (LEO), rather than in the GEO. Details about the CYGNSS orbit and a comparison to that of the GPS constellation are given in Table I. This measurement geometry allows for the sampling of the transmitted signal throughout the main beam portion of the GPS antenna pattern. Like the previous work mentioned above, the GPS satellite transmit pattern has been reasonably assumed to be purely RHCP, and we expect to be measuring the RHCP component of the CYGNSS receive GPS antenna. The link equation for the received signal power is inverted to determine the receive antenna pattern on each CYGNSS satellite. In addition, the GPS transmit antenna gain pattern can also be determined by the inversion of the link equation. The retrieval procedure, validation with prelaunch chamber measurements, and impact on CYGNSS Level 1 calibration are detailed in the following sections.

Portions of this article appeared previously in the first author's Ph.D. thesis [21].

II. SPACEBORNE ANTENNA RANGE MEASUREMENTS

A. Constellations of GPS and CYGNSS

The GPS constellations of satellites are all in the medium earth orbit (MEO) at 20 180-km altitude. There are currently 31 operational satellites consisting of four different SV designs (referred to as block types), including Blocks IIR, IIR-M, IIF, and III. For Block IIR and IIR-M SVs, there are two antenna designs used.

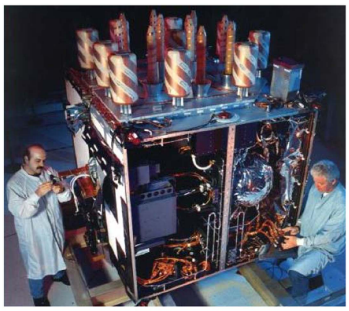
The CYGNSS constellations of eight satellites are all in the LEO at 520-km altitude. They share a common orbit plane, and the orbit period is approximately 95 min. Each spacecraft carries a navigation receiver connected to a zenith-mounted antenna that receives direct GPS L1 coarse/acquisition (C/A) code signals for navigation. Two science receivers connected to nadir-mounted antennas also receive reflected GPS signals from the earth surface for remote sensing applications. While calibration of these nadir GPS antennas is important for a number of science applications, it is not the focus of this work.

The CYGNSS zenith navigation antenna is a half-wave dipole patch. Its gain pattern was measured in an anechoic chamber prior to launch while mounted on a satellite mock-up. Those measurements revealed that the pattern is affected by coupling and multipath from nearby structures on the spacecraft. The measured pattern cannot be assumed to be an accurate representation of the on-orbit patterns due to mechanical tolerances and limits on repeatability that are associated with the final assembly of the spacecraft. For these reasons, the on-orbit patterns may differ from the prelaunch pattern and from one another.

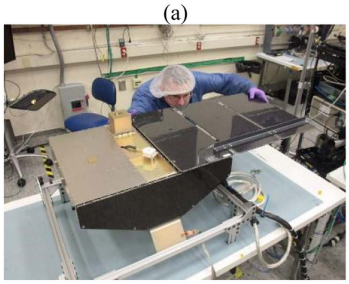
Examples of the GPS transmit antenna (Block IIR, legacy antenna panel) and the CYGNSS zenith antenna are shown in Fig. 1(a) and (b), respectively.

B. Spaceborne Antenna Measurement Range

The CYGNSS provides a unique opportunity for precise determination of the GPS transmit and CYGNSS receive antenna gain patterns, which includes the effects of satellite structures on their patterns. Both the GPS and CYGNSS satellites have precisely known positions and orientations; they are in the orbit well above any tropospheric propagation effects, and they are free of environmental multipath. At



(a)



(b)

Fig. 1. Example photos of the antennas being measured in this work. (a) GPS transmit antenna (Block IIR) [15]. (b) CYGNSS zenith GPS receive antenna (white square radome) during satellite assembly.

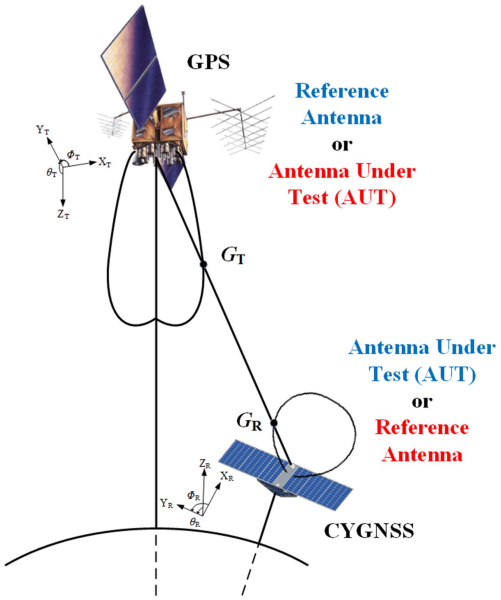


Fig. 2. Spaceborne antenna range measurement system formed by constellations of GPS and CYGNSS satellites (note: not to scale).

these altitudes, the only propagation effect that could potentially impact the measurement is ionospheric scintillation. When GPS receivers are used in the LEO, ionospheric effects must still be considered since, although scintillation tends to be generated at the maximum electron density at approximately 350 km where irregularities occur, the ionosphere extends from 50 km to more than 1000 km [22]. Models, such as the global ionospheric scintillation model, can be used to estimate the scintillation index (S4) and predict the degradation of the amplitude of the received GPS signal. In [22], an example of ionospheric impact is characterized on a receiver in the typical LEO, showing that about 60% of the total electron content (TEC) is above the receiver, and the depth of the scintillation fading ranges from 2 dB to more than 20 dB, depending on the solar activity. Nonetheless, these ionospheric events are expected to be rare, and the results here are aggregated over several years of measurements. The method of analysis used effectively averages the ionospheric effects over this time period.

In this sense, measurements between the two satellites form an ideal "spaceborne antenna range." It provides a unique opportunity for precise determination of the GPS transmit and CYGNSS receive antenna gain patterns, which includes the effects of satellite structures on their patterns. Fig. 2 depicts the antenna measurement setup. From an antenna range perspective, the GPS satellite antenna can be viewed as the illuminating source and the CYGNSS antenna, as the antenna under test (AUT). By reciprocity, the GPS satellite antenna can also be viewed as the AUT if the CYGNSS antenna pattern is known. Several sources have reported bounds on the cross-pol [left-handed circular polarization (LHCP)] component of the GPS satellite antennas as –15 dB or less. Indeed, the official GPS interface control document (ICD) specifies a cross-pol axial ratio value of less than ∼1 dB [14]. Consequently, for this work, it is assumed that the GPS satellite antenna is purely RHCP. Although the CYGNSS zenith receive antenna is expected to have a significant LHCP pattern component (as shown in Section V-B), it is only the RHCP component that is expected to be measured using our approach. While any LHCP component of the GPS transmitted signal is expected to be small and not significant, if that is, in fact, not the case, then the derived CYGNSS receive antenna patterns presented here should not be viewed as pure RHCP patterns but rather as composite polarization patterns.

C. Angular Sampling of the GPS Satellite Antenna Pattern

The use of the orbiting CYGNSS receivers is an attractive alternative to ground stations when it comes to achieving robust angular sampling of the GPS satellite antenna pattern. If we assume that the GPS satellite attitude has a fixed yaw angle relative to its orbit coordinate frame, then the angular sampling of a single fixed ground station would be very limited. Reconstructing the GPS antenna pattern using a global GPS receiver network [23] is feasible, but it may require additional efforts in system calibration and signal processing. The highly repeatable 12-h GPS orbit results in measurements made at a fixed ground location that cut through nearly identical slices of the GPS pattern day after day and month after month. This is illustrated in Fig. 3(a), which shows the location in the GPS antenna coordinate system of all the samples made by a ground-based receiver over a 100-day period. In the figure, the radial coordinate is the angular distance from the antenna boresight, and the azimuthal coordinate is the azimuthal angle about the boresight direction, with 0° referenced to

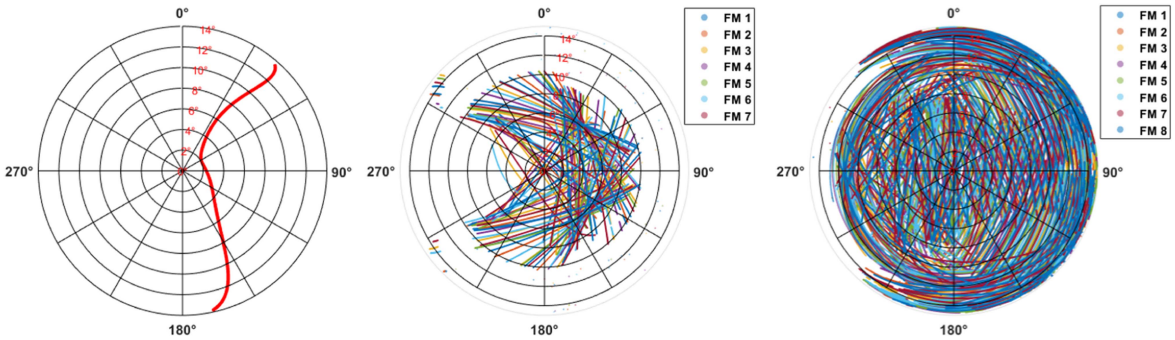


Fig. 3. Location in the GPS antenna coordinate system of gain pattern measurements made by (a) a ground-based receiver over 100 days, (b) eight CYGNSS satellites in one day, and (c) eight CYGNSS satellites in one week.

the $+X$-axis in the GPS satellite reference frame. A more detailed description of the coordinate system can be found in [15]. For the results shown in Fig. 3(a), the receiver was located in Ann Arbor, MI, USA, and the GPS satellite is space vehicle number (SVN) 54, but the results are similar for any fixed location and specific SV. It should be noted, however, that the GPS satellites are known to regularly adjust their yaw state in relation to the Sun [24]. While this yaw information is not publicly available, such variations could result in an improved angular sampling of the GPS antenna pattern beyond that illustrated here. Nonetheless, the variation would still be less than if the receiver were instead located on a LEO satellite.

Compared to using a ground-based receiver to calibrate GNSS antennas, there is a distinct advantage in angular sampling when using a spaceborne receiver [25]. Fig. 3(b) shows the location of all the samples made of a single GPS antenna pattern (in the GPS antenna coordinate system) by the eight CYGNSS satellites in one day, and Fig. 3(c) shows the sampling distribution after one week. The GPS pattern is much more fully sampled by the CYGNSS satellites in one week than the ground-based system was able to in 100 days. For the work presented here, we use approximately two years of samples by the constellation of CYGNSS satellites for even better pattern coverage. The spaceborne antenna range system provides nearly gap-free measurements of the GPS satellite antenna pattern over all the azimuth angles and out to an off-boresight angle of $\sim$15.2°. The earth horizon is located at $\sim$13.8° in the GPS satellite antenna coordinate system, and the CYGNSS is able to measure the GPS satellite transmit gain pattern as it extends into the LEO space service volume due to its 520-km orbit altitude.

D. Sampling Density of GPS Satellite and CYGNSS Satellite Antenna Patterns

In this work, antenna patterns are estimated using measurements made by the spaceborne antenna range over a long time interval to further improve the sampling distribution, to allow for the detection of outlier data samples, and to average out the effects of measurement noise. Both the GPS and CYGNSS antennas are jointly estimated, and they can each be treated as the AUT at different stages of the analysis.

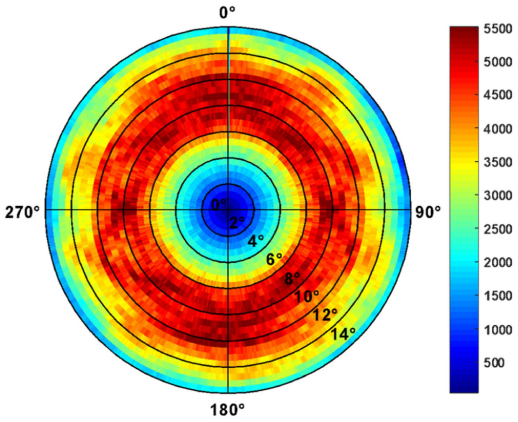


Fig. 4. Sampling density over GPS satellite's transmit antenna pattern using approximately two years of data.

Fig. 4 shows the sampling density for a particular GPS satellite antenna from 2018 day of year (DOY) 213 to 2020 DOY 182 using measurements from all eight CYGNSS satellites. The sampling density is shown in the GPS satellite antenna coordinate system, and it accounts for the orientation of the GPS satellite. Changes in the GPS yaw state [24], [26] are accounted for using the GNSS-Inferred Positioning System-X (GipsyX) software [27] licensed by the NASA Jet Propulsion Laboratory. In the figure, the angular resolution of sampling density is 0.5° × 0.5°, and the color map denotes the number of samples in each bin.

Fig. 5 shows the sampling density of a single CYGNSS antenna pattern in its coordinate system, using all data from the same time period as Fig. 4. Measurements in this figure are accumulated over a subset of GPS SVNs: 41, 43, 44, 45, 46, 51, and 56. This particular subset of GPS SVs is used because: 1) they correspond to older block types, which have been found to exhibit less variability in their transmit power level than the more recent block types [28], [29], [30]; and 2) their antenna patterns have less azimuthal variability, according to the published patterns in [15]. The angular resolution in Fig. 5 and in the estimated CYGNSS antenna patterns is 1° × 1°.

The distribution of samples of CYGNSS patterns is much less uniform than that of the GPS patterns. Samples

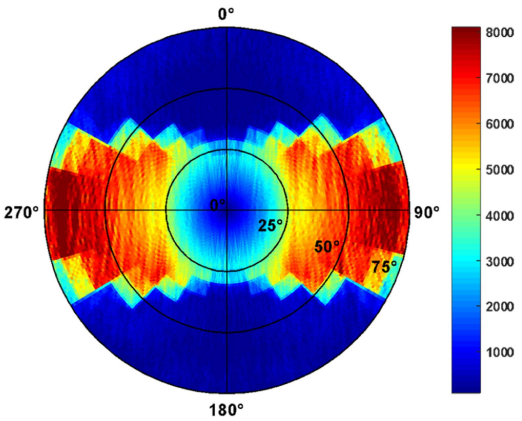


Fig. 5. Sampling density over CYGNSS satellite's receive antenna pattern using approximately two years of data.

are concentrated in the vicinity of azimuthal angles 90° and 270°, which correspond to the starboard and port directions relative to the forward motion of the CYGNSS satellites. This uneven sampling density results from a property of the CYGNSS GPS receivers, which records signals from GPS transmitters for which the signal reflected from the earth surface enters the nadir science antenna in its main beam. The science antennas are fan beams pointed in the spacecraft's starboard and port directions. Only measurements of direct signals received by the zenith antenna that correspond to reflected signals received by the nadir antennas are downlinked to the ground. This restriction on the distribution of samples of the zenith pattern means that, unlike with the GPS patterns, its gain cannot be determined uniformly across the entire main beam. Fortuitously, it is only in the portions of the main beam that are well sampled that accurate antenna gain knowledge is required for purposes of CYGNSS science data calibration.

E. Equations for On-Orbit Received Power

The received power referenced to the output port of the CYGNSS zenith antenna, P_R, can be determined from P_Z, the calibrated power at the input port of the receiver, by correcting for the gain of the zenith low-noise amplifier (LNA), G_{LNA}, according to

$$P_R = \frac{P_Z}{G_{\mathrm{LNA}}\left(T_{\mathrm{LNA}}\right)} \tag{1}$$

where T_{LNA} is the temperature of the zenith LNA, G_{LNA} is calculated using a prelaunch lookup table of gain versus physical temperature, and P_Z is converted from raw counts to power in watts based on the hardware calibration experiment described in our previous studies [10], [11].

The Friis transmission equation expresses the relationship between the received power and the gain of transmit and receive antennas according to

$$P_R = \frac{\lambda^2}{(4\pi R)^2} P_T G_T\left(\theta_T, \phi_T\right) G_R\left(\theta_R, \phi_R\right) \tag{2a}$$

$$G_R\left(\theta_R, \phi_R\right) = \frac{(4\pi R)^2}{\lambda^2} \frac{P_R}{P_T G_T\left(\theta_T, \phi_T\right)} \tag{2b}$$

$$G_T\left(\theta_T, \phi_T\right) = \frac{(4\pi R)^2}{\lambda^2} \frac{P_R}{P_T G_R\left(\theta_R, \phi_R\right)} \tag{2c}$$

where G_T is the gain of the GPS transmit antenna, G_R is the gain of the zenith receiver antenna, R is the distance from the transmitter to the receiver, λ is the wavelength for GPS L1 signals, P_T is the transmit power of the GPS satellite, θ_T is the GPS off-boresight angle from the nadir ($+Z_T$), ϕ_T is the GPS azimuthal angle that is counterclockwise around the boresight referenced to the $+X_T$-axis, θ_R is the CYGNSS off-boresight angle from its boresight ($+Z_R$), and ϕ_R is the CYGNSS azimuthal angle that is counterclockwise around the boresight referenced to the $+X_R$-axis, as depicted in the coordinate systems in Fig. 2.

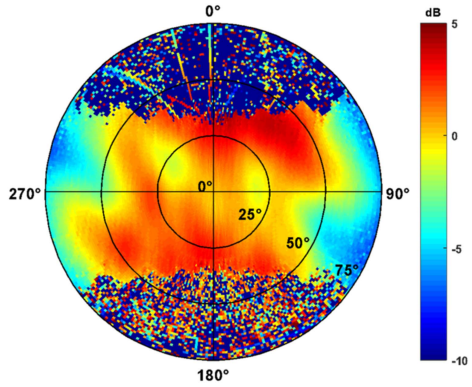
Equations (2b) and (2c) are used to compute the gain of the GPS transmit antenna and the CYGNSS receive antenna in the following sections.

III. Estimation of CYGNSS and GPS Satellite Antenna Patterns

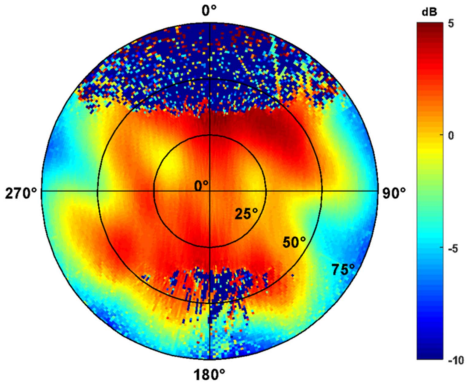
Either the GPS antenna or the CYGNSS antenna can be considered the AUT. Depending on which one it is, one or the other of (2b) or (2c) is used to estimate the gain. Therefore, the estimation of one of the gain patterns presupposes knowledge of the other one. Both the patterns can be estimated sequentially. The CYGNSS receive pattern, G_R, is estimated first by assuming that the published prelaunch GPS pattern is G_T. Next, the GPS pattern is estimated by assuming that the CYGNSS pattern is G_R that was just determined. If the new GPS pattern is identical to the prelaunch pattern, then the estimation process is complete. As will be shown below, this turns out not to be the case, and an iterative procedure will be developed, which can jointly estimate both the patterns.

A. Estimation of CYGNSS Zenith Antenna Patterns

There are eight CYGNSS spacecraft, which are designated flight model (FM) 1–8. Although all spacecraft and GPS antennas are meant to be identical, small differences in each antenna combined with differences in the deployment of satellite solar panels results in significant gain pattern differences. For this reason, each receive antenna pattern is determined independently. For each one, the pattern can be estimated using many different GPS SVs as the transmitter. We use the subset of seven GPS SVs noted earlier, because their transmit power level P_T is most stable over time. Examples of the resulting G_R patterns for FM 1 using SVNs 43 and 46 are shown in Fig. 6(a) and (b), respectively. Several characteristics of the two patterns are noteworthy. Both are well sampled over the azimuthal ranges 75–105° and 255–285° for reasons discussed earlier. The two gain patterns are generally consistent in these two sectors. Outside of the sectors, the sampling density varies due to differences in the individual orbits of the GPS satellites, and some angular regions are sampled better by one SV

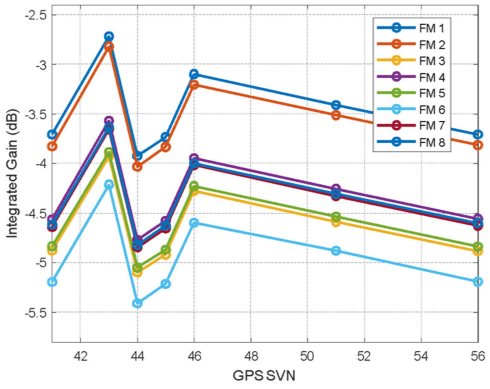


(a)

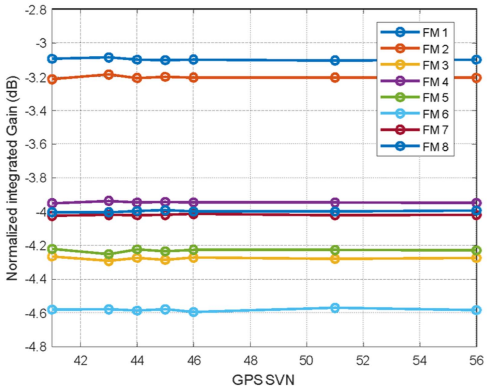


(b)

Fig. 6. Example of the retrieved zenith antenna gain pattern (FM 1) using signals from (a) GPS SVN 46 and (b) SVN 43.



(a)



(b)

Fig. 7. Normalized integrated gain G_{NI} versus GPS SVN for eight FMs. (a) Raw calculation. (b) Bias removed.

than the other. For this reason, it is desirable to combine together patterns estimated using multiple SVs to create a single well-sampled composite pattern. Before doing so, it is prudent to test whether the patterns are consistent with one another within the angular region in which they overlap.

The average value of G_R over the two well-sampled sectors is considered individually for each FM derived from each SV. This value, referred to as the normalized integrated gain, G_{NI}, is given by

$$G_{\mathrm{NI}} = \sum_{\theta_i=25^\circ}^{70^\circ} \left[\sum_{\phi_i=75^\circ}^{105^\circ} G_R(\theta_i, \phi_i) \sin\theta_i + \sum_{\phi_i=255^\circ}^{285^\circ} G_R(\theta_i, \phi_i) \sin\theta_i \right] \Delta\theta \Delta\phi \quad (3)$$

where θ_i and ϕ_i are the off-boresight and azimuthal angles, respectively, and the discretized average is computed over ϕ_i within $\pm 15^\circ$ of the port and starboard directions and over θ_i within 25–70°. $\Delta\theta$ and $\Delta\phi$ are the resolution over off-boresight and azimuth. These are the two sectors with consistently high sampling density for all the SVs. N is the total number of pixels used.

A comparison of G_{NI} for the eight CYGNSS FMs and seven GPS SVs is shown in Fig. 7(a). The different colors indicate different FMs, and the x-axis is the GPS SVN. A shift in the average gain is evident between SVs that is consistent across all the FMs. The most likely cause of the shift is errors in the assumed GPS transmit power levels of the individual SVs. The values used for P_T are based on previous measurements made by a ground-based GPS power monitor system, as reported in [17] and [18]. The shifts in G_{NI} for a fixed FM as SVN is varied represent differences in the error in P_T. It is not possible with this analysis to determine absolute values for each P_T, but it is possible to adjust their individual values so that any remaining error is common to all seven SVs. This is done by assuming that the average value of P_T across all seven SVs is correct and then rescaling the individual values so that G_{NI} is consistent. The result is shown in Fig. 7(b), which is computed in the same way as in Fig. 6(a) after the individual values of P_T have been adjusted. Once the P_T adjustment has been made, the individual G_R patterns derived from each SV can now be combined together into a single pattern. The result is shown in Fig. 8 for FM 1, where the center is the boresight, and circles represent different off-boresight angles. Similar G_R patterns are computed in the same way for each FM.

B. Estimation of GPS Satellite Antenna Patterns

The antenna gain pattern G_T for GPS satellites can be estimated using (2c), when the eight FM patterns derived in the previous subsection are assumed for G_R. Similarly,

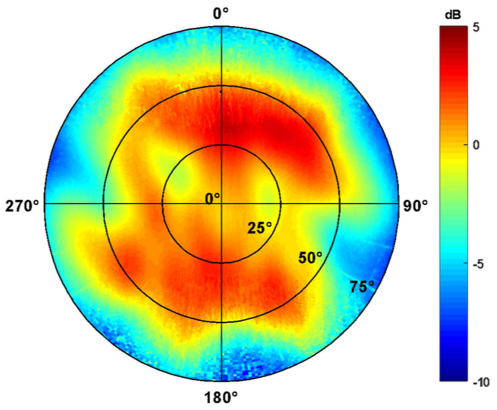
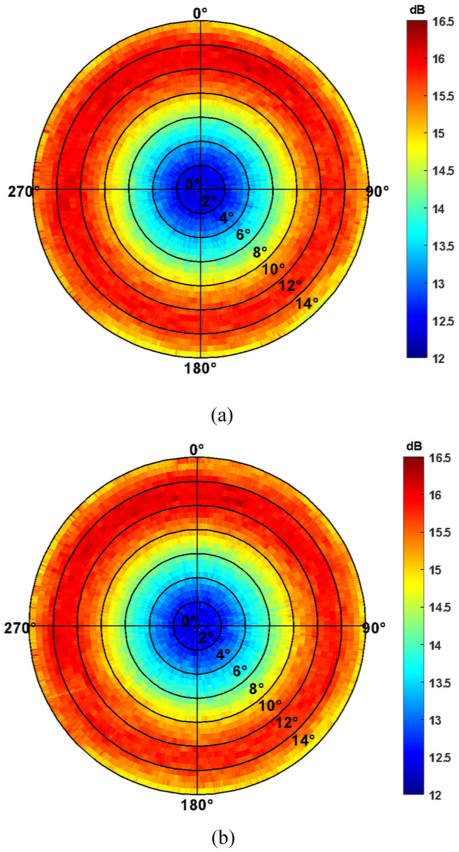


Fig. 8. Example of the retrieved zenith gain pattern (FM 1) using seven SVs.



(a)

(b)

Fig. 9. Example of the retrieved GPS gain pattern (SVN 56) using signals from (a) CYGNSS FM 1 and (b) FM 2.

G_T is retrieved using individual FM's measurements, as the examples given in Fig. 9(a) and (b). The retrieved patterns of SVN 56 using measurements made by FM 1 and FM 2 are generally similar, while having minor differences. This further confirms the correctness of the normalization process in Section III-A.

Then, the GPS antenna patterns retrieved from eight FMs' measurements are combined together by a weighting average to estimate the final pattern, as the example of SVN 56 shown in Fig. 10. The computed GPS antenna pattern is considered reliable at off-boresight angles of less than 12°. Above this angle, the low gain of the CYGNSS receive antenna reduces the received signal strength significantly.

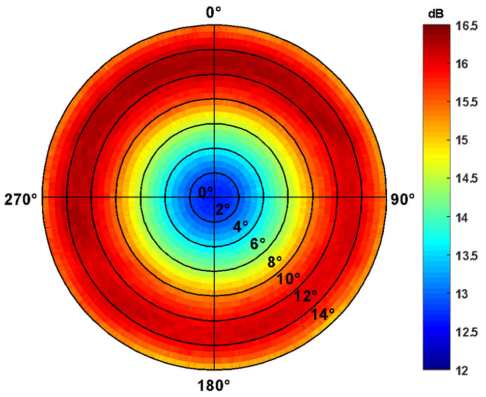
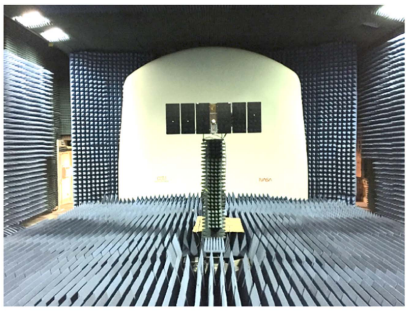
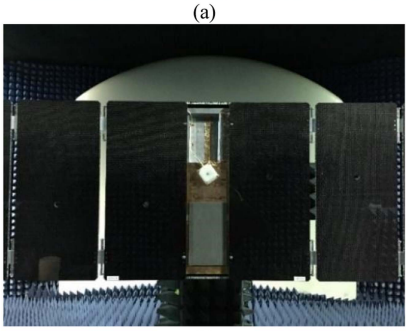


Fig. 10. Example of the retrieved GPS gain pattern (SVN 56) using signals from all eight CYGNSS FMs.



(a)



(b)

Fig. 11. (a) Compact range measurement of the CYGNSS zenith antenna. (b) Close-up view of the antenna (small white square) on the approximate satellite mock-up.

IV. VALIDATION

A. CYGNSS Zenith Antenna Pattern

In order to provide validation of our measured CYGNSS zenith antenna pattern, anechoic chamber measurements were performed. Measurements took place in a compact antenna measurement test range at The Ohio State University ElectroScience Laboratory, as shown in Fig. 11. For these measurements, the antenna was mounted on an approximate CYGNSS satellite mock-up. These measured patterns are referred to as the prelaunch patterns. Dual-polarized measurements were made. The RHCP component is used for validation, while the LHCP component is included to provide additional information to the reader. Additional tests using different configurations were performed, and the results indicate that the platform has a significant effect on the CYGNSS antenna gain pattern. Therefore, considering the differences between the FM and the test model, as

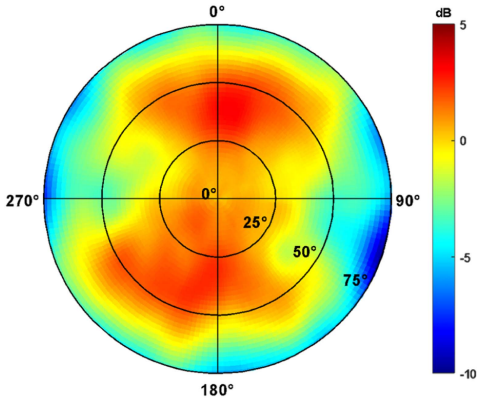


Fig. 12. Scaled prelaunch measured pattern using a satellite mock-up.

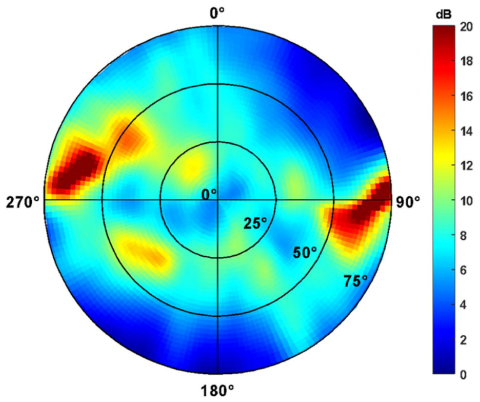


Fig. 13. Measured cross-pol isolation (dB) for prelaunch patterns with a satellite mock-up.

well as the disparities among the flight antennas, these chamber measurements alone should not be used for science calibration but should be improved upon with on-orbit measurements.

Fig. 12 shows the prelaunch measured pattern of the CYGNSS antenna mounted on a spacecraft mock-up. Note that the prelaunch measured pattern is rescaled to remove a calibration offset (2.5 dB), which is believed to originate from the GPS receiver instrument aboard the satellite. It is clear that the prelaunch and retrieved patterns in Fig. 8 are qualitatively very similar, which gives us confidence about the accuracy of the pattern estimation method in general. However, there are significant differences between them as well. It should be noted that the CYGNSS zenith antenna is a miniaturized single-layer patch antenna, which we would expect to have a smooth and uniform pattern. However, on the spacecraft, the antenna is mounted in a narrow channel between the edges of the large solar panels that results in significant near-field coupling of the antenna, platform multipath, and detuning of the patch. These effects are evident in the rapid variations in the measured antenna pattern in Fig. 12 as well as in its striking pattern asymmetry. In this configuration, the pattern of the antenna is very sensitive to small variations in the satellite structure or in manufacturing differences between different antennas. Thus, we expect there to be significant differences between the prelaunch measurements on the approximate satellite mock-up and the on-orbit measurements using the real satellite platforms. These differences support the notion that antenna patterns should be independently determined for each of the CYGNSS spacecraft while on-orbit in their operational environment, and this is the primary motivation for this work.

The cross-pol isolation of the prelaunch CYGNSS antenna pattern measurements is shown in Fig. 13. This is the difference (in dB) between the RHCP and LHCP pattern components. The observed cross-pol isolation is quite poor, with most angles being between 6–12 dB and some angles being as little as 3 dB. It is expected that this is due to the effects of the coupling and scattering of the satellite platform on the otherwise well-designed patch antenna. If one focuses on angles with the highest measurement density (see Fig. 5), one can interpret the average cross-pol isolation as being approximately 10 dB over the set of measurements used to estimate the GPS satellite antenna patterns. Nonetheless, as mentioned earlier, since the GPS satellite transmit antenna has been reported as having a cross-pol isolation of more than 20 dB, we can conclude that the on-orbit approach is measuring the RHCP components of both the transmit and in situ receive antenna patterns (that is, the receive antenna pattern that incorporates all the effects of the receiver satellite platform).

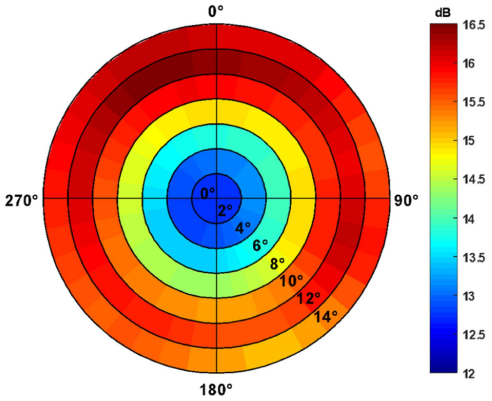


Fig. 14. Published GPS antenna patterns of SVN 56 [15].

B. GPS Satellite Antenna Gain Pattern

Fig. 14 shows the published prelaunch pattern for GPS SVN 56 published in [15]. The retrieved pattern in Fig. 10 shows azimuthal asymmetry features, which are generally consistent with those of the prelaunch pattern. However, because of its much higher angular resolution, small features can be seen in the retrieved pattern that cannot be resolved by the prelaunch one.

Fig. 15 plots the difference between the prelaunch G_T pattern and the one derived here. Note that the published prelaunch patterns are only available with a coarse $2^\circ \times 10^\circ$ resolution so the retrieved pattern has been smoothed to that same resolution to compute the difference. It shows clear signs of structural differences between the two antenna patterns, as opposed to unstructured random differences

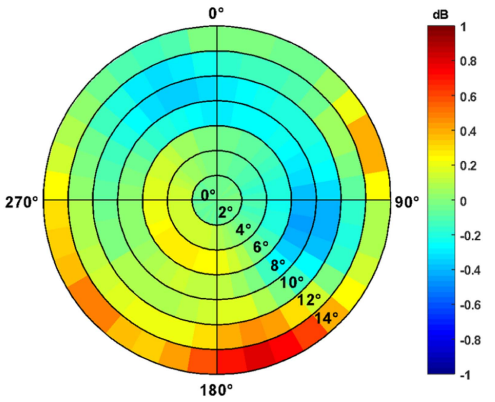


Fig. 15. Difference between the published prelaunch pattern and the retrieved pattern for SVN 56.

that might be attributed to measurement noise. To minimize uncertainty in antenna patterns, an iterative solution is being considered next, which updates estimates of G_R and G_T at each iteration. The objective is for the iterative process to converge to a pair of patterns that are mutually consistent with the measured values of P_R, as stipulated by the relationship in (3). This will be studied as our future work.

V. DISCUSSION

A. Summary of Results

Table II summarizes the limited knowledge of the GPS and CYGNSS antenna patterns prior to the work presented here and the improvements that have been made. Specifically: 1) for CYGNSS antennas, eight estimated gain patterns were characterized in their operational environment, compared with only one prelaunch measured pattern using a single crude CYGNSS satellite mock-up; and 2) for GPS antennas, more than 31 GPS patterns are estimated precisely ($0.5° \times 0.5°$) and accurately when the antennas are mounted on the satellites and in their operational environment, compared with only 20 published prelaunch measured patterns with rather coarse ($2° \times 10°$) angular resolution.

Note that the two sets of antenna patterns need to be validated with independent measurement, e.g., received signals observed by calibrated ground-based GNSS systems or other spaceborne GNSS receivers.

B. Impact on CYGNSS Level 1 Calibration

These antenna gain patterns have been applied to the official version 3.0, 3.1, and 3.2 Level 1 calibration and science data processing algorithms of the NASA CYGNSS mission, specifically on the dynamic EIRP calibration approach descripted in [11]. The CYGNSS zenith antenna gain patterns are used to calibrate the CYGNSS direct signal and to estimate the GPS EIRP in the direction of the CYGNSS spacecraft E_Z. Then, the GPS EIRP in the direction of the specular reflection point E_S is estimated by using the zenith-to-specular ratio functions, which are derived from the retrieved GPS antenna gain patterns. E_S serves as a key input to the Level 1 calibration algorithm described in [8] and [9].

TABLE II
Improvement of Antenna Pattern Characterization

Antenna	Before	After
GPS	20 prelaunch measured patterns with limited angular resolution ($2° \times 10°$)	More than 31 estimated patterns with the antenna in its operational environment ($0.5° \times 0.5°$)
CYGNSS	One prelaunch measured pattern using a spacecraft mock-up	Eight estimated patterns in its operational environment

Two independent approaches, root of sum of squares analysis and Monte Carlo simulation, are used for error analysis, and they agree well with both estimating ~0.32-dB relative error. This reduces the 0.4-dB error term of GPS EIRP in v2.1 Level 1 calibration [9] by approximately 20%. Besides, the 0.4-dB error does not consider flex power events, which can introduce greater than 2-dB errors due to the variation of GPS transmit power; thus, the improvement could be significantly larger.

The dynamic EIRP calibration algorithm has been proved to be able to instantaneously detect and correct for power fluctuations in all the GPS transmitters and significantly reduces errors due to the azimuthal asymmetry of the GPS antenna gain patterns. It allows observations with Block IIF transmitters (approximately 37% of the entire dataset) to be included in the standard data products and further improves the calibration quality [11].

VI. SUMMARY AND FUTURE WORK

This article presents an approach that estimates RHCP gain patterns of GPS satellite and CYGNSS antennas using spaceborne measurement. Actual on-orbit data are used to determine the patterns in their operational environment. This cannot be practically achieved prior to launch using ground-based systems. GPS antenna patterns are produced with high angular resolution covering the complete on-earth solid angle plus a small off-earth portion near the limb. The new GPS and CYGNSS patterns have been incorporated into the science data processing algorithms used by the CYGNSS mission and have resulted in improved calibration performance [11].

Future work will focus on: 1) revisiting the end-to-end zenith calibration experiment; 2) identifying calibration error sources including: a) time variations of the GPS transmit power; b) aging of the CYGNSS receiver system, which could introduce time-dependent errors in calibration of the received power, P_R; and c) RF interference in the CYGNSS received signal (also possibly time dependent); 3) making appropriate empirical corrections and quality control to received signals; 4) developing an iterative retrieval process to minimize retrieval uncertainty; 5) analyzing the systematic differences between retrieved antenna patterns; 6) performing absolute calibration and error analysis of antenna patterns for all the GPS transmitters; and 7) validating the retrieved patterns with independent measurements.

ACKNOWLEDGMENT

The authors would like to thank the editor and reviewers for their insightful and invaluable comments toward improving this article.

REFERENCES

[1] B. Hofmann-Wellenhof, H. Lichtenegger, and J. Collins, *Global Positioning System: Theory and Practice*, 5th ed. Vienna, Austria: Springer-Verlag, 2001.

[2] P. Misra and P. Enge, *Global Positioning System: Signals, Measurements, and Performance*, 2nd ed. Lincoln, MA, USA: Ganga-Jamuna Press, 2001.

[3] V. U. Zavorotny, S. Gleason, E. Cardellach, and A. Camps, "Tutorial on remote sensing using GNSS bistatic radar of opportunity," *IEEE Geosci. Remote Sens. Mag.*, vol. 2, no. 4, pp. 8–45, Dec. 2014.

[4] S. Gleason, S. Lowe, and V. Zavorotny, "Remote sensing with bistatic GNSS reflections," in *GNSS Applications and Methods*, S. Gleason and D. Gebre-Egziabher, Eds., Norwood, MA, USA: Artech House, 2009, pp. 399–436.

[5] S. Gleason, "Remote sensing of ocean, ice and land surfaces using bistatically scattered GNSS signals from low earth orbit," Ph.D. dissertation, Dept. Appl. Phys., Univ. Surrey, Guildford, U.K., 2006.

[6] C. S. Ruf et al., "The CYGNSS nanosatellite constellation hurricane mission," in *Proc. IEEE Int. Geosci. Remote Sens. Symp.*, 2012, pp. 214–216.

[7] C. Ruf et al., "CYGNSS: Enabling the future of hurricane prediction," *IEEE Geosci. Remote Sens. Mag.*, vol. 1, no. 2, pp. 52–67, Jun. 2013.

[8] S. Gleason, C. S. Ruf, M. P. Clarizia, and A. J. O'Brien, "Calibration and unwrapping of the normalized scattering cross section for the cyclone global navigation satellite system," *IEEE Trans. Geosci. Remote Sens.*, vol. 54, no. 5, pp. 2495–2509, May 2016.

[9] S. Gleason, C. S. Ruf, A. J. Orbrien, and D. S. McKague, "The CYGNSS level 1 calibration algorithm and error analysis based on on-orbit measurements," *IEEE J. Sel. Topics Appl. Earth Observ. Remote Sens.*, vol. 12, no. 1, pp. 37–49, Jan. 2019.

[10] T. Wang, C. Ruf, S. Gleason, B. Block, D. McKague, and A. O'Brien, "A real-time EIRP level 1 calibration algorithm for the CYGNSS mission using the zenith measurements," in *Proc. IEEE Int. Geosci. Remote Sens. Symp.*, 2019, pp. 8725–8728.

[11] T. Wang et al., "Dynamic calibration of GPS effective isotropic radiated power for GNSS-reflectometry Earth remote sensing," *IEEE Trans. Geosci. Remote Sens.*, vol. 60, 2022, Art. no. 580051.

[12] F. M. Czopek and S. Shollenberger, "Description and performance of the GPS block I and II l-band antenna and link budget," in *Proc. 6th Int. Tech. Meeting Satell. Division Inst. Navigat.*, 1993, pp. 37–43.

[13] M. C. Moreau, F. H. Bauer, J. R. Carpenter, E. P. Davis, G. W. Davis, and L. A. Jackson, "Preliminary results of the GPS flight experiment on the high Earth orbit AMSAT-OSCAR 40 spacecraft," in *Proc. 25th Annu. Amer. Astronaut. Soc. Guid. Control Conf.*, 2002, pp. 45–59.

[14] "GPS technical references." Accessed: Dec. 14, 2023. [Online]. Available: https://www.navcen.uscg.gov/gps-technical-references

[15] W. A. Marquis and D. L. Reigh, "The GPS block IIR and IIR-M broadcast L-band antenna panel: Its pattern and performance," *NAVIGATION: J. Inst. Navigat.*, vol. 62, no. 4, pp. 329–347, Winter 2015.

[16] P. Steigenberger, S. Thoelert, and O. Montenbruck, "GNSS satellite transmit power and its impact on orbit determination," *J. Geodesy*, vol. 92, no. 6, pp. 609–624, Jun. 2018.

[17] T. Wang, C. Ruf, S. Gleason, B. Block, D. McKague, and D. Provost, "Development of GPS constellation power monitor system for high accuracy calibration/validation of the CYGNSS L1B data," in *Proc. IEEE Int. Geosci. Remote Sens. Symp.*, 2017, pp. 1008–1011.

[18] T. Wang, C. S. Ruf, B. Block, D. S. McKague, and S. Gleason, "Design and performance of a GPS constellation power monitor system for improved CYGNSS L1b calibration," *IEEE J. Sel. Topics Appl. Earth Observ. Remote Sens.*, vol. 12, no. 1, pp. 26–36, Jan. 2019.

[19] T. Wang, C. Ruf, B. Block, and D. McKague, "Characterization of the transmit power and antenna pattern of the GPS constellation for the CYGNSS mission," in *Proc. IEEE Int. Geosci. Remote Sens. Symp.*, 2018, pp. 4011–4014.

[20] J. E. Donaldson, J. J. K. Parker, M. C. Moreau, D. E. Highsmith, and P. D. Martzen, "Characterization of on-orbit GPS transmit antenna patterns for space users," *NAVIGATION: J. Inst. Navigat.*, vol. 67, no. 2, pp. 411–438, 2020.

[21] T. Wang, "Engineering calibration and physical principles of GNSS-reflectometry for Earth remote sensing," Ph.D. dissertation, Dept. Elect. Eng., , Univ. Michigan, Ann Arbor, MI, USA, 2021.

[22] A. Camps, H. Park, G. Foti, and C. Gommenginger, "Ionospheric effects in GNSS-reflectometry from space," *IEEE J. Sel. Topics Appl. Earth Observ. Remote Sens.*, vol. 9, no. 12, pp. 5851–5861, Dec. 2016.

[23] G. Allende-Alba, S. Thoelert, and S. Caizzone, "Gain pattern reconstruction of GPS satellite antennas using a global receiver network," *NAVIGATION: J. Inst. Navigat.*, vol. 69, no. 3, 2022, Art. no. 530.

[24] Y. E. Bar-Sever, "A new model for GPS yaw attitude," *J. Geodesy*, vol. 70, pp. 714–723, Nov. 1996.

[25] T. Wang, C. Ruf, B. Block, D. McKague, and S. Gleason, "Characterization of GPS L1 EIRP: Transmit power and antenna gain pattern," in *Proc. 31st Int. Tech. Meeting Satell. Division Inst. Navigat.*, 2018, pp. 2879–2890.

[26] J. Kouba, "A simplified yaw-attitude model for eclipsing GPS satellites," *GPS Solutions*, vol. 13, no. 1, pp. 1–12, 2009.

[27] W. Bertiger et al., "GipsyX/RTGx, a new tool set for space geodetic operations and research," *Adv. Space Res.*, vol. 66, no. 3, pp. 469–489, 2020.

[28] P. Steigenberger, A. Hauschild, S. Thoelert, and R. B. Langley, "US air force puts more power into GPS block IIR-M C/A-code," *GPS World*, vol. 28, no. 4, pp. 8–9, Apr. 2017.

[29] S. Thoelert, A. Hauschild, P. Steigenberger, R. B. Langley, and F. Antreich, "GPS IIR-M L1 transmit power redistribution: Analysis of GNSS receiver and high-gain antenna data," *NAVIGATION: J. Inst. Navigat.*, vol. 65, no. 3, pp. 423–430, 2018.

[30] P. Steigenberger, S. Thoelert, and O. Montenbruck, "Flex power on GPS Block IIR-M and IIF," *GPS Solutions*, vol. 23, no. 1, pp. 1–12, 2019.



Tianlin Wang (Senior Member, IEEE) received the B.E. degree in electrical engineering from the East China University of Science and Technology, Shanghai, China, in 2009, the M.S. degree in radio physics from Fudan University, Shanghai, in 2012, and the Ph.D. degree in electrical engineering from the University of Michigan, Ann Arbor, MI, USA, in 2021.

He is currently a President's Postdoctoral Scholar with the Department of Electrical and Computer Engineering and ElectroScience Laboratory, The Ohio State University, Columbus, OH, USA. His research interests include wave propagation and scattering, microwave remote sensing, microwave measurements, and radio frequency circuits.

Dr. Wang is the recipient of the 2018 IEEE Mikio Takagi Student Prize, an Outstanding Student Presentation Award at the 2018 AGU Fall Meeting, the 2020 Richard F. and Eleanor A. Towner Prize for Distinguished Academic Achievement and Distinguished Leadership Award from the University of Michigan, and the 2021 Ernest K. Smith USNC-URSI Student Prize. He is also the recipient of the 2020 President's Postdoctoral Scholars Program Fellowship from the Ohio State University and the 2021 Mistletoe Research Fellowship from the Momental Foundation. He is a Co-chair of the Modeling in Remote Sensing Technical Committee of the IEEE Geoscience and Remote Sensing Society (GRSS), a Member of the Chapters Committee of the IEEE GRSS, and a Member of the Young Professionals Committee of the IEEE GRSS. He is a Member of Tau Beta Pi, Eta Kappa Nu, the American Geophysical Union, and the Institute of Navigation, and an Early Career Member of the Commission F of the U.S. National Committee for the Union Radio Scientifique Internationale.



Christopher S. Ruf (Life Fellow, IEEE) received the B.A. degree in physics from Reed College, Portland, OR, USA, in 1982, and the Ph.D. degree in electrical and computer engineering from the University of Massachusetts at Amherst, Amherst, MA, USA, in 1987.

He is currently the Frederick Bartman Collegiate Professor of Climate and Space Science with the University of Michigan, Ann Arbor, MI, USA, and the Principal Investigator of the NASA Cyclone Global Navigation Satellite System Mission. He was with Intel Corporation, Santa Clara, CA, USA; Hughes Space and Communication, San Diego, CA; the NASA Jet Propulsion Laboratory, Pasadena, CA; and Penn State University, State College, PA, USA. His research interests include global navigation satellite system reflectometry remote sensing, microwave radiometry, atmosphere and ocean geophysical retrieval algorithm development, and sensor technology development.

Dr. Ruf was the recipient of the 1997 IEEE TGRS Best Paper Award, the 1999 IEEE Resnik Technical Field Award, the 2006 IGARSS Best Paper Award, the 2014 IEEE GRSS Outstanding Service Award, the 2017 AIAA SmallSat Mission of the Year Award, and the 2020 University of Michigan Distinguished Faculty Achievement Award. He is a former Editor-in-Chief for IEEE TRANSACTIONS ON GEOSCIENCE AND REMOTE SENSING. He was on the Editorial Board of *Radio Science*, *Journal of Atmospheric and Oceanic Technology*, and *Nature Scientific Reports*. He is a Member of the American Geophysical Union, the American Meteorological Society, and the Commission F of the Union Radio Scientifique Internationale.



Andrew J. O'Brien received the B.S., M.S., and Ph.D. degrees in electrical engineering from The Ohio State University, Columbus, OH, USA, in 2005, 2007, and 2009, respectively.

He has worked in the area of adaptive global navigation satellite system (GNSS) antenna arrays and precision GNSS receiver algorithms for over a decade. He was a Research Scientist with the ElectroScience Laboratory, Department of Electrical and Computer Engineering, The Ohio State University, Columbus, OH, USA, where his primary research focused on spaceborne GNSS remote sensing using Cyclone Global Navigation Satellite System (CYGNSS), TechDemoSat-1, and soil moisture active passive. His research interests include GNSS antenna arrays, antenna electronics, electromagnetic simulation, and radar systems.

Dr. O'Brien was a Member of the CYGNSS Science Team and supported the development of CYGNSS end-to-end simulator and CYGNSS engineering activities.



Scott Gleason (Senior Member, IEEE) received the B.S. degree in electrical and computer engineering from the State University of New York at Buffalo, Buffalo, NY, USA, in 1991, the M.S. degree in engineering from Stanford University, Stanford, CA, USA, in 1999, and the Ph.D. degree in applied physics from the University of Surrey, Surrey, U.K., in 2007.

He is currently the President of Daaxa LLC, Boulder, CO, USA, specializing in global navigation satellite system instruments, calibration, and remote sensing applications. He is a Co-Investigator on the science team and an Instrument Scientist for the NASA Cyclone Global Navigation Satellite System mission. He has worked in the areas of astronautics, remote sensing, and global navigation satellite systems for more than 20 years, including at the NASAs Goddard Space Flight Center, Greenbelt, MD, USA; Stanford's GPS Laboratory Stanford; Surrey Satellite Technology Limited, Guildford, U.K.; Concordia University, Montreal, QC, Canada; Southwest Research Institute, San Antonio, TX, USA; the University Corporation for Atmospheric Research, Boulder; and the National Oceanography Centre, Southampton, U.K.



Darren S. McKague (Member, IEEE) received the Ph.D. degree in astrophysical, planetary, and atmospheric sciences from the University of Colorado, Boulder, CO, USA, in 2001.

He was a Systems Engineer with Ball Aerospace, Broomfield, CO, and with Raytheon, Waltham, MA, USA, and a Research Scientist with Colorado State University, Fort Collins, CO. He is currently an Associate Research Scientist with the Department of Climate and Space Sciences and Engineering, University of Michigan, Ann Arbor, MI, USA. His work has focused on remote sensing with emphases on the development of spaceborne microwave remote sensing hardware, microwave remote sensor calibration techniques, and mathematical inversion techniques for geophysical retrievals. His experience with remote sensing hardware includes systems engineering for several advanced passive and active instrument concepts and the design of the calibration subsystem on the Global Precipitation Mission (GPM) Microwave Imager as well as the development of calibration and intercalibration techniques for the GPM constellation. His algorithm experience includes the development of a near-real-time algorithm for the joint retrieval of water vapor profiles, temperature profiles, cloud liquid water path, and surface emissivity for the Advanced Microwave Sounding Unit, Colorado State University, and the development of the precipitation rate, precipitation type, sea ice, and sea surface wind direction algorithms for the risk reduction phase of the Conical scanning Microwave Imager/Sounder.



Bruce P. Block received the B.S. degree in electrical engineering from the University of Michigan, Ann Arbor, MI, USA, in 1975.

He is currently a Lead Engineer in Research with the Space Physics Research Laboratory, College of Engineering, University of Michigan, Ann Arbor, MI, where he developed hardware and software for ground testing of the Cyclone Global Navigation Satellite System Delay–Doppler Mapping Instrument. In addition to his interests in global navigation satellite system technology for geodesy and remote sensing, he has, over the course of 40 years, developed numerous electromechanical designs for spaceborne mass spectrometry, Langmuir probe, and gas chromatography instruments in collaboration with the NASA's Goddard Space Flight Center, Greenbelt, MD, USA; the Jet Propulsion Laboratory, Pasadena, CA, USA; the Marshall Space Flight Center, Huntsville, AL, USA; the Johns Hopkins University Applied Physics Laboratory, Laurel, MD; and the European Space Agency, Paris, France.



Anthony Russel received the B.S. degree in computer science engineering from Michigan State University, East Lansing, MI, USA, in 2014.

He is currently a Member of the Engineering Staff with the Space Physics Research Laboratory, College of Engineering, University of Michigan, Ann Arbor, MI. His research interests include algorithm development and large-scale data processing.

Mr. Russel is a Member of the Science Operations Center for the Cyclone Global Navigation Satellite System mission.